*J Neuropathol Exp Neurol*
Vol. 76, No. 10, October 2017, pp. 874–882
doi: 10.1093/jnen/nlx072

ORIGINAL ARTICLE

# Aggressive Behavior in Silent Subtype III Pituitary Adenomas May Depend on Suppression of Local Immune Response: A Whole Transcriptome Analysis

Timothy E. Richardson, DO, PhD, Zhong-Jian Shen, PhD, Mohammed Kanchwala, MS, Chao Xing, PhD, Alexander Filatenkov, MD, Ping Shang, MS, Samuel Barnett, MD, Zahidur Abedin, PhD, James S. Malter, MD, Jack M. Raisanen, MD, Dennis K. Burns, MD, Charles L. White, MD, and Kimmo J. Hatanpaa, MD, PhD

**Abstract**

Silent subtype III pituitary adenomas (SS-3) are clinically nonfunctional adenomas that are more aggressive in terms of invasion and risk of recurrence than their conventional null cell counterparts. We previously showed that these tumors can be distinguished by immunohistochemistry based on the identification of a markedly enlarged and fragmented Golgi apparatus. To understand the molecular correlates of differential aggressiveness, we performed whole transcriptome sequencing (RNAseq) on 4 SS-3 and 4 conventional null cell adenomas. The genes that were highly upregulated in all the SS-3 adenomas included 2 secreted proteins involved in the suppression of T-lymphocyte activity, i.e., *ARG2* (multiple testing adjusted $p_{adj} = 1.5 \times 10^{-3}$) and *SEMA3A* ($p_{adj} = 3.3 \times 10^{-3}$). Highly downregulated genes in all the SS-3 adenomas included *HLA-B* ($p_{adj} = 3.3 \times 10^{-6}$), suggesting reduced antigen presentation by the adenoma to cytotoxic T-cells. Quantitative RT-PCR of these genes performed on the adenoma samples supported the RNAseq results. We also found a relative decrease in the overall concentration of T-lymphocytes in the SS-3 tumors. These results suggest that SS-3 adenomas actively suppress the immune system and raise the possibility that they may be treatable with immune checkpoint inhibitors or nonspecific cancer immunotherapies.

From the Department of Pathology (TER, Z-JS, AF, PS, JSM, JMR, DKB, CLW, KJH); Eugene McDermott Center for Human Growth and Development, (MK, CX); Department of Bioinformatics (CX); Department of Clinical Sciences (CX) and Department of Neurosurgery, University of Texas Southwestern Medical Center, Dallas, Texas (SB); and PrimBio Research Institute, LLC, Exton, Pennsylvania (ZA)

Send correspondence to: Kimmo J. Hatanpaa, MD, PhD, Department of Pathology, University of Texas Southwestern Medical Center, 5323 Harry Hines Blvd., Dallas, TX 75390; E-mail: kimmo.hatanpaa@utsouthwestern.edu

Financial support: Portions of these studies were paid for by UTSW Department of Pathology intradepartmental trainee research grant 2100202200 (awarded to Timothy E. Richardson) and NIH grants P01HL088594 (to James S. Malter) and UL1TR001105 (to Chao Xing).

Conflict of interest: The authors have no duality or conflicts of interest to declare.

Supplementary Data can be found at http://www.jnen.oxfordjournals.org.

**Key Words:** ARG2, HLA-B, Null cell adenoma, Pituitary adenoma, SEMA3A, Silent subtype III, Transcriptome sequencing.

## INTRODUCTION

First identified and characterized ultrastructurally in the 1980's, silent subtype III pituitary adenomas (SS-3) account for <2% of all pituitary adenomas (1, 2). It has recently been suggested that these tumors represent a poorly differentiated member of the Pit-1 family of pituitary adenomas, which includes growth hormone (GH)-, thyroid stimulating hormone (TSH)-, and prolactin (PRL)-secreting adenomas (3). These SS-3 adenomas have been shown to be significantly more aggressive than their more indolent null cell (NC) counterparts in terms of frequency of recurrence and invasion into bone or into the surrounding cavernous sinus (2, 4–8). Classically, SS-3 was differentiated from conventional null cell adenomas only by electron microscopy findings, most importantly an enlarged and multicentric Golgi apparatus, similar to that seen in hormone-producing adenomas, in the setting of a nonfunctional adenoma (1, 2, 5). We have recently shown that the diagnosis can be made by visualizing the enlarged and tortuous Golgi apparatus with an immunohistochemical stain specific to the Golgi apparatus, GLG-1/MG-160 (4). The enlarged Golgi apparatus raises the possibility that these tumor cells are producing a yet unknown secreted gene product that could potentially be contributing to the increased aggressive behavior attributed to SS-3 adenomas or be used as a biomarker for diagnosis and/or prognosis.

We evaluated a small cohort of SS-3 adenomas compared them to a group of conventional null cell adenomas by whole-transcriptome sequencing to search for upregulated or downregulated gene products, focusing on cancer-related proteins and secreted proteins. In this study, the SS-3 pituitary adenomas showed a marked increase of the level of mRNA of secreted gene products linked to immunosuppression and T-cell regulation including *ARG2* and *SEMA3A*, as well as a marked decrease of *HLA-B* expression relative to a

conventional null cell pituitary adenoma control group. The alterations in the expression of all 3 of these genes have been linked to worse outcomes in other types of tumors (9–14). These data could partially explain the increased aggressiveness seen with the SS-3 subtype as well as provide additional therapeutic options targeting these immunomodulatory proteins (2, 4, 5).

## MATERIALS AND METHODS

### Case Selection and Clinical Review

We identified 4 cases with the diagnosis silent subtype III pituitary adenoma using a SNOMED database search at our institution. This diagnosis had been made at the time of the original neuropathologic work-up from 2013 to 2015 primarily based on the clinical impression of a nonsecreting pituitary tumor combined with the pathology finding of a markedly enlarged Golgi apparatus, as identified by GLG-1/MG-160 immunohistochemistry in the absence of any significant immunoreactivity to pituitary hormones, according to our previously published method (4) (Supplementary Data Fig. S1). In addition, we randomly selected 4 cases with the diagnosis of "null cell adenoma," from 2013 to 2015. All available clinical history, physical examination findings, imaging results, laboratory results, operative reports, pathology findings, and subsequent follow-up encounters were reviewed and relevant data are reported in Table 1. The study was performed in accordance with a protocol approved by the Institutional Review Board of the University of Texas Southwestern Medical Center (IRB STU 022011-081).

### Immunohistochemistry

Four-μm-thick sections of formalin-fixed paraffin-embedded (FFPE) tissue underwent heat-induced epitope retrieval using CC1 (Ventana Medical Systems, Inc., Tucson, AZ), a tris-based buffer at an 8–8.5 pH followed by immunohistochemical staining with the polyclonal rabbit antibody antiMG-160 (GLG-1) (Sigma Life Science Prestige Antibodies, St. Louis, MO), on either the Ventana Benchmark XT or Ventana Benchmark Ultra automated stainer, using Ventana UltraView Universal DAB Detection Kit. Similar immunostaining was also performed using mouse monoclonal antisynaptophysin (Ventana), rabbit polyclonal antiPRL (Ventana), rabbit polyclonal antiadrenocorticotrophic hormone ([ACTH] Ventana), rabbit polyclonal antiGH (Ventana), mouse monoclonal antiTSH (Dako North America, Inc., Carpinteria, CA), mouse monoclonal antifollicle stimulating hormone (Ventana), mouse monoclonal antiluteinizing hormone (Dako), mouse monoclonal antiKi-67 (Dako), and rabbit monoclonal antiCD3 (Ventana) antibodies. The Ki-67/MIB-1 labeling indices were quantified using a Glasgow cell counting graticule at 400× magnification (15).

### RNA Purification From Paraffin Sections

Formalin-fixed, paraffin-embedded tissue blocks were sectioned at a thickness of 10 μm. Freshly cut sections were placed in 2 mL microcentrifuge tubes and deparaffinized by vortexing in xylene, followed by centrifugation. The xylene was removed and the sections were washed in 100% molecular biology-grade ethanol. The residual ethanol was removed by evaporation. The RNA was then purified with an RNeasy FFPE RNA extraction kit (QIAGEN, Redwood City, CA, Cat. No. 73504), according the manufacturer's protocol.

### Whole Transcriptome Sequencing and Analysis

Library Preparation: RNA was purified from 10 FFPE sections per case as described above. cDNA libraries were constructed using Ion Ampliseq Transcriptome Human Gene Expression Kit (Life Technologies, Carlsbad, CA, Cat. No. A26325) and the manufacturer's recommended protocol. Briefly, 100 ng of total RNA was reverse transcribed at 42 °C for 30 minutes. After reverse transcription, the cDNA was amplified by PCR using Ion Ampliseq Transcriptome Human Gene Expression Core Panel primers that amplified the specific targets (Step 1: 99 °C for 2 minutes; Step 2: 99 °C for 15 seconds, 60 °C for 16 minutes for 16 cycles; Step 3: Hold at 10 °C). Next, the primers were partially digested as directed. Following the partial digestion of primers, adapters and bar codes were ligated to the cDNA. The cDNA was purified using AMPure XP reagent and recommended protocol. The purified cDNA libraries were amplified by PCR using 1X Library Amp Mix and 2 μL of 25X Library Amp Primers with the conditions as follows: Step 1: 98 °C for 2 minutes; Step 2: 98 °C for 15 seconds, 64 °C for 1 minute; Steps 2–3 for 5 cycles. The amplified cDNA libraries were purified using Nucleic Acid binding beads, binding buffers and run on Agilent 2100 Bioanalyzer to determine the yield and size distribution of each library.

Templating, Enrichment, and Sequencing: Approximately 100 pM of pooled barcoded libraries were used for templating using Life Technologies Ion PI™ Hi-Q™ OT2 200 Kit (Cat. No. A26434) and manufacturers recommended protocol. One hundred pM of pooled libraries were combined and 25 μl of each sample was loaded onto the Ion Chef. The Ion Chef templates, enriches, and loads the sample onto a P1 chip, and then after 15 hours the Chef pauses so that QC can be performed on the unenriched samples. After the pause, the beads were isolated and quality assessment was performed on Qubid instrument to determine the percent of beads that were polyclonal. After polyclonal assessment, the Ion Chef resumed running and loaded the samples onto a P1 chip. The loaded chip was then placed into an Ion Proton sequencer and the run was started using an Ion torrent Ampliseq transcriptome run plan that was configured based on type of library, species, number of run flows required, type of plug-in required, adapter-trimming as well as other parameters specific to the Ampliseq transcriptome run.

Alignment and Data Analysis: Fastq files were checked for quality using fastqc v0.11.2 (http://www.bioinformatics.babraham.ac.uk/projects/fastqc) and fastq screen v0.4.4 (http://www.bioinformatics.babraham.ac.uk/projects/fastq_screen) and were quality trimmed using fastq-mcf (ea-utils/1.1.2-806) (16). Trimmed fastq files were mapped to hg19 (UCSC version from iGenomes) using TopHat (17);

**TABLE 1.** Summary of the Relevant Clinical, Radiologic and Laboratory Findings, As Well As Subsequent Follow-Up Data

| Patient | Age | Gender | History | Imaging | Hormone Levels | Immunoreactivity | Proliferative Index | Diagnosis | Outcome |
|---|---|---|---|---|---|---|---|---|---|
| 1 | 67 | Female | Six year history of slowly growing pituitary adenoma | 5.6 × 4.1 × 3.8 cm mixed solid/cystic enhancing sellar mass; noninvasive | No abnormalities | Approximately 7% of tumor cells positive for FSH | MIB-1: 0.6%; 0 mitoses per 10 HPF | Null cell | No recurrence (at 24 months) |
| 2 | 44 | Male | Hyponatremia and history of low testosterone | 3.1 × 2.6 × 2.2 cm cystic/nodular enhancing sellar mass; noninvasive | Decreased T by patient history | Negative | MIB-1: 1.3%; 0 mitoses per 10 HPF | Null cell | No recurrence (at 18 months) |
| 3 | 63 | Male | History of persistent headaches | 1.9 × 1.8 × 1.6 cm homogeneously enhancing sellar mass; noninvasive | No abnormalities | Negative | MIB-1: 0.9%;0 mitoses per 10 HPF | Null cell | No recurrence (at 18 months) |
| 4 | 73 | Male | History of visual disturbances | 2.0 × 1.9 × 1.7 cm homogeneously enhancing sellar mass; noninvasive | No abnormalities | 2% of tumor cells positive for LH | MIB-1: 0.5%; 0 mitoses per 10 HPF | Null cell | No recurrence (at 2 months) |
| 5 | 41 | Female | Subtotal pituitary adenoma resection in 2005 at OSH | 2.4 × 1.6 × 1.6 cm homogeneously enhancing sellar mass invading into left cavernous sinus | No abnormalities | 0.1% of tumor cells positive for prolactin | MIB-1: 2.6%; 0 mitoses per 10 HPF | SS-3 | Recurrent/residual within 1 year; radiation therapy (CyberKnife) |
| 6 | 62 | Female | One year of bitemporal hemianopsia | 6.9 × 6.5 × 5.4 cm homogeneously enhancing sellar mass invading into bilateral cavernous sinuses | No abnormalities | Negative | MIB-1: 2.5%;0 mitoses per 10 HPF | SS-3 | Recurrent/residual tumor; repeat surgery6 months later then subsequent recurrence; radiation therapy |
| 7 | 60 | Male | History of low testosterone | 2.1 × 1.5 × 1.5 cm heterogeneously enhancing sellar mass; noninvasive | Decreased T by patient history | Negative | MIB-1: 2.1%;0 mitoses per 10 HPF | SS-3 | No recurrence (at 18 months) |
| 8 | 26 | Male | Three previous resections of pituitary adenomas: 2011, 2012, 2013 at OSH | 3.3 × 3.0 × 2.9 cm homogeneously enhancing sellar mass invading into the left cavernous sinus | No abnormalities | 0.5% of tumor cells positive for GH and prolactin | MIB-1: 3.5%; 1 mitosis per 10 HPF | SS-3 | No recurrence (at 4 months) |

duplicates were marked using picard-tools (v1.127 https://broadinstitute.github.io/picard/); read counts were generated using featureCounts (18); and differential expression analysis was performed using edgeR (19). Differentially expressed gene heat maps were clustered by hierarchical clustering using R (http://www.R-project.org) (Fig. 1).

## Quantitative RT-PCR Confirmation of Whole Transcriptome Sequencing Results

RNA was purified from two 10-µm FFPE sections from each case as described above. cDNA Quantitative PCR was performed with a SYBR PCR master mix with the primers purchased from OriGene Technologies, Inc. (Rockville, MD). *ARG2* forward sequence: 5′-CTGGCTTGATGAAAA GGCTCTCC-3′; reverse sequence: 5′-TGAGCGTGGATTCA CTATCAGGT-3′. *HLA-B* forward sequence: 5′-CTGCTGT GATGTGTAGGAGGAAG-3′; reverse sequence: 5′-GCTGT GAGAGACACATCAGAGC-3′. *SEMA3A* forward sequence: 5′-GGTGCCTTATCAAGGAAGAGTCC-3′; reverse sequence: 5′-TACATGGCTGGATGACTTCTTGC-3′. An ABI 7500 thermocycler (Applied Biosystems, Foster City, CA) was used for 45 cycles of PCR. ΔCT calculates the differences between target CT values and the normalizer (housekeeping genes GAPDH and β-actin) (20) for each sample: ΔCT = CT (target) − CT (normalizer). The comparative ΔΔCT calculates the differences between each sample ΔCT value and the baseline ΔCT. The comparative expression level (fold changes) was obtained transforming the logarithmic values to absolute values using $2^{-\Delta\Delta CT}$. All data from null cell pituitary adenoma samples was normalized to fold change = 1 (21).

## Pathway Analysis

All genes with significant differential expression between SS-3 and NC groups ($p_{adj} \leq 0.05$; n = 213 genes) were used for pathway analysis with QIAGEN's Ingenuity Pathway Analysis tool (QIAGEN, http://www.qiagen.com/ingenuity). The resulting full list of the 287 enriched canonical pathways along with the p-values, gene ratios, *Z*-scores, and pathway component molecules are reported in Supplementary Data Table S1.

## Relative Quantification of Lymphocytes

The relative extents of tumor infiltrating lymphocytes (TILs) were determined by visual inspection of 5 randomly selected areas of 1 antiCD3-stained section of each case from this study, as well as 10 null cell and 10 silent subtype III cases from our previous study (4). The following approximate grades were designated: − (completely absent); + (rare TILs or lymphocytes restricted to adjacent tissue); ++ (widespread lymphocytes infiltrating into 5%–25% of the area of the tumor); and +++ (lymphocytes infiltrating into ≥25% of the tumor) (22).

## Statistics

For RNAseq data, false discovery rate (FDR) control procedure was performed, and the adjusted p values ($p_{adj}$)

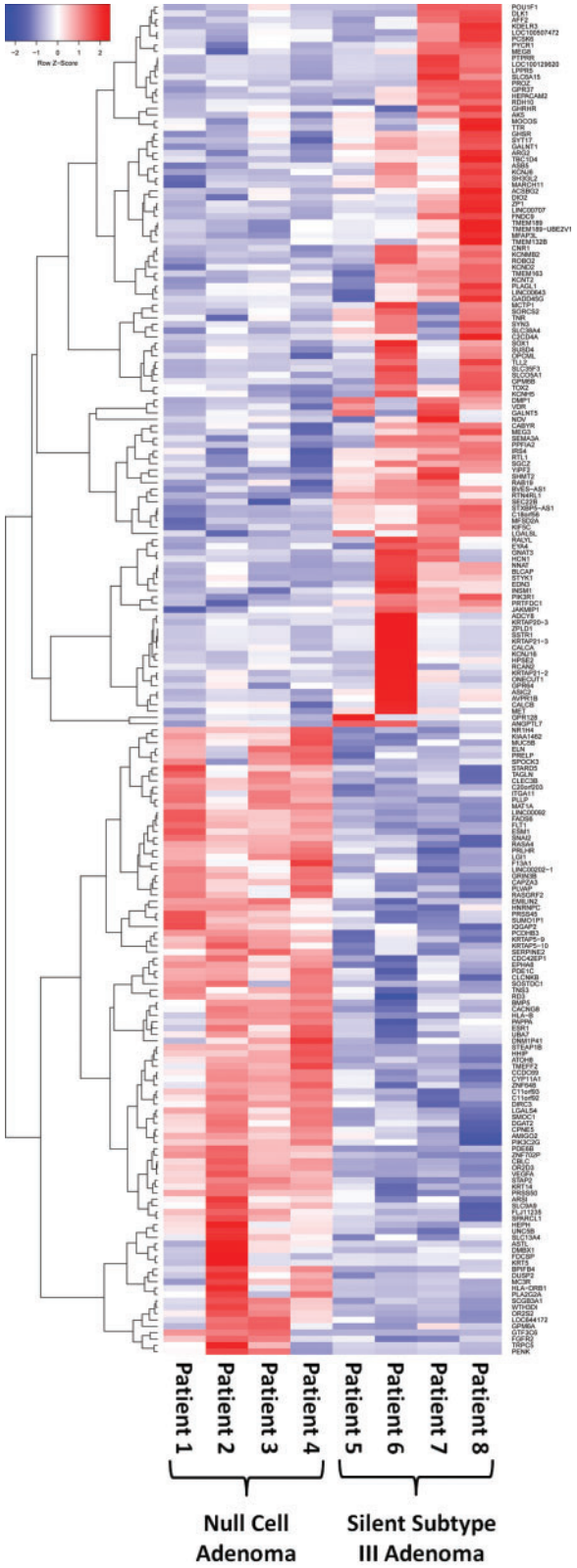


**FIGURE 1.** Heat map showing different patterns of gene expression in SS-3 and conventional null cell adenomas. The rows represent the most significantly upregulated and downregulated genes. Scale bar: normalized fold change.

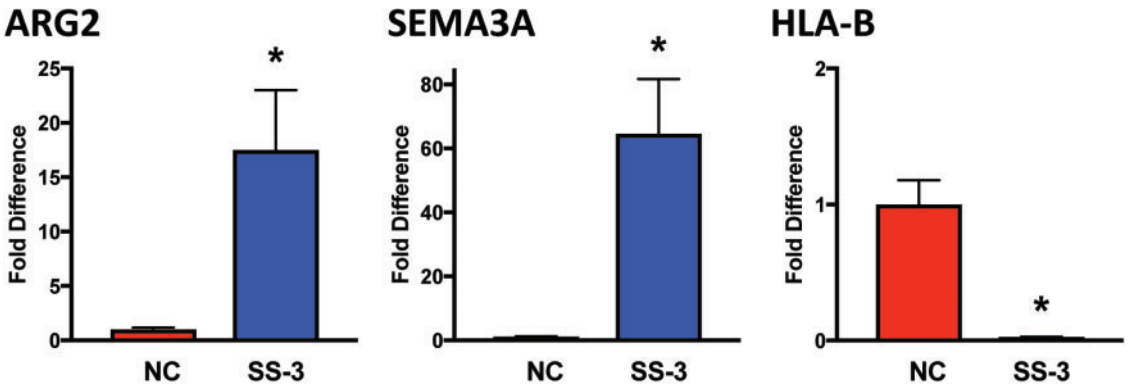


**FIGURE 2.** Relative mRNA levels of *ARG2*, *SEMA3A*, and *HLA-B* between SS-3 and conventional null cell pituitary adenomas. Error bars = 1 SD. *$p < 0.01$.

<0.05 were considered significant. For TIL analysis, nonparametric Mann–Whitney *U*-testing was performed (http://vassarstats.net).

## RESULTS

### Clinical and Pathological Features

As previously reported, the SS-3 pituitary adenomas generally had more invasive characteristics than the conventional null cell adenomas (4). While none of the null cell cases were invasive according to the previously established definition of invasion (8), 3 of the SS-3 tumors included herein invaded into the cavernous sinuses with ≥50% encasement of at least 1 cavernous internal carotid artery. In addition, while no NC tumor showed evidence of recurrence, 2 of the SS-3 tumors subsequently recurred; and 1 patient had undergone 3 previous resections for similar pituitary adenomas before being seen at our institution. There was a significant difference in the MIB-1 proliferative index between these 2 groups with the NC group measuring 0.83% ± 0.36% and the SS-3 group measuring 2.68% ± 0.59% ($p = 0.0017$). No significant difference was noted in the patient age, 61.8 ± 12.5 years and 47.3 ± 17.4 years in the NC and SS-3 groups, respectively ($p = 0.22$). Similarly, there was no difference in tumor size between the 2 groups, (2.93 ± 1.98 cm and 3.68 ± 2.21 cm in greatest dimension in the NC and SS-3 groups, respectively, $p = 0.63$).

### Altered Expression of Genes Related to Immune Surveillance Mechanisms in SS-3 Pituitary Adenomas

Compared with the conventional null cell pituitary adenoma group, SS-3 adenomas had significantly increased levels of *ARG2* (17.5-fold increase; $p_{adj} = 1.5 \times 10^{-3}$) and *SEMA3A* (64.6-fold increase; $p_{adj} = 3.3 \times 10^{-3}$) mRNA, as well as significantly decreased levels of *HLA-B* (212-fold decrease; $p_{adj} = 3.3 \times 10^{-6}$; all p-values adjusted for multi-hypothesis testing) (Fig. 2). Of all genes identified by this method, these genes are among the most statistically significant and among those with the greatest fold changes (Fig. 3). These data are consistent with observations in other tumor types where similar changes have been linked with decreased T-cell proliferation and infiltration, increased tumor growth, increased lymph node and distant organ metastases, and decreased response to therapy. The results for the 3 genes were confirmed by qRT-PCR analysis, normalized to β-actin mRNA levels in each sample ($p < 0.01$).

### Other Differences in Whole-Transcriptome Sequencing mRNA Levels

Whole transcriptome differential expression analysis demonstrated the following additional genes differentially expressed at the FDR level of 0.05: a 95.6-fold increase in *GHRHR*, a 60.4-fold increase in *HEPACAM2*, a 64.9-fold increase in *GHSR*, a 59.3-fold increase in *GADD45G*, a 33.2-fold increase in *NNAT*, and a 25.7-fold increase in *MET* (Fig. 1). In addition, there was a 55.6-fold decrease in *LGI1*, a 32.3-fold decrease in *BMP5*, an 18.5-fold decrease in *Emilin2*, a 13.9-fold decrease in *PIK3C2G*, a 11.3-fold decrease in *DIRC3*, a 10.7-fold decrease in *HLA-DRB1* (Fig. 3), and a 5.2-fold decrease in *TAGLN*.

### Pathway Analysis

The pathway analysis suggests that several canonical signaling pathways known to be associated with cellular proliferation, T-lymphocyte regulation and inhibition, as well as angiogenesis in various cancers are also activated in aggressive pituitary adenomas such as SS-3 adenomas (Table 2).

### Decreased Numbers of CD3-Positive Lymphocytes in SS-3 Tumors

We evaluated the numbers of CD3-positive TILs in cases 1–8, as well as an additional 10 NC cases and 10 SS-3 cases from our previous cohort (4). All NC and the majority of SS-3 cases had some lymphocytes in the tumor and in the tissue surrounding the tumor, which suggests that the adenomas can elicit a T-cell response. The SS-3 cases had absent to rare T-cells sparsely scattered through the tissue, while there were variably increased T-cell numbers in the null cell tumors (Fig. 4; Table 3). There was a significant difference between the SS-3 and NC groups in terms of TIL numbers by Mann–Whitney

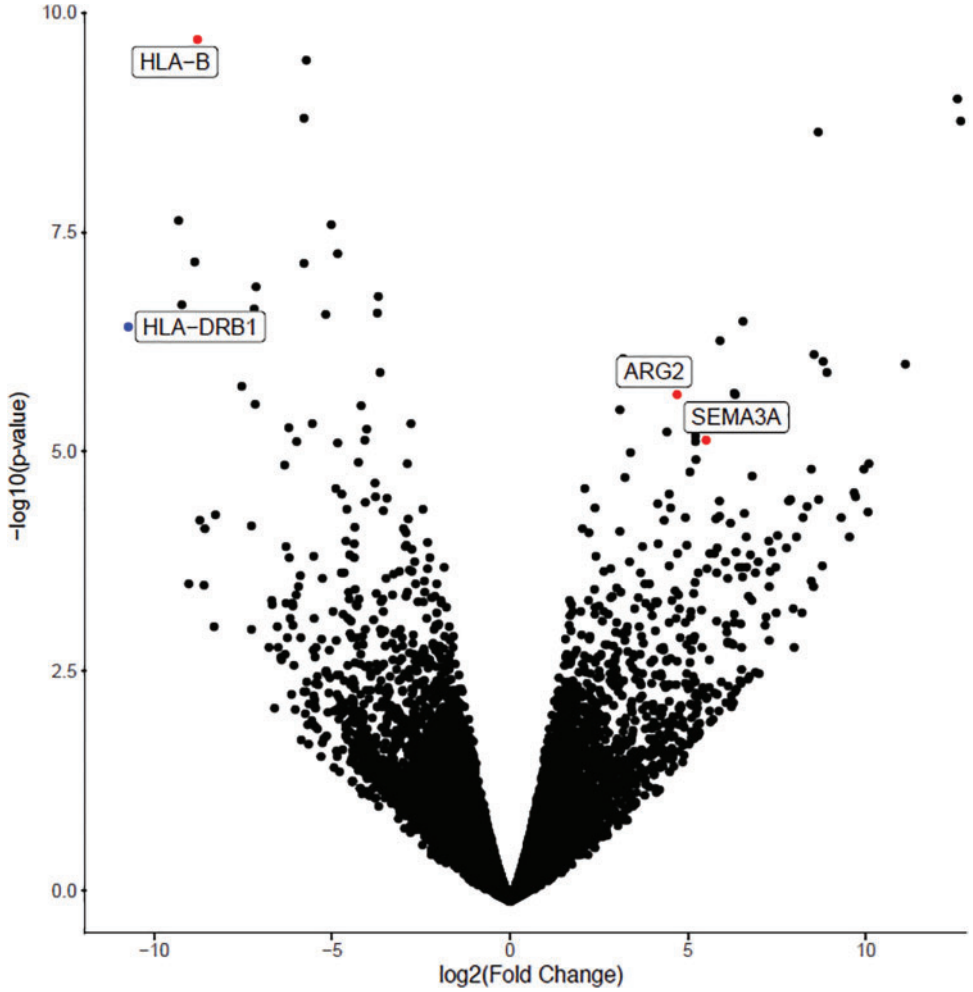


**FIGURE 3.** Volcano plot demonstrating genes with markedly different levels of expression between the 2 groups, with genes of interest highlighted by red labeling (confirmed by qRT-PCR) and blue labeling (qRT-PCR not performed).

*U*-test ($p = 0.006$), supporting our hypothesis that SS-3 adenomas may inhibit T-cell response in the tumor microenvironment.

## DISCUSSION

Having previously confirmed the significantly worse prognosis associated with SS-3 adenomas compared with conventional null cell adenomas (4), we performed RNAseq on a subset of our SS-3 adenoma cases to identify genes that could potentially explain this difference in outcome. RNAseq demonstrated a clear difference in overall RNA expression profiles between the 2 tumor types (Fig. 1) and identified a number of genes that could be involved with aggressive behavior in SS-3 adenomas. Notably, *ARG2* and *SEMA3A*, both of which are involved in the regulation of T-cell proliferation and function within the tumor microenvironment (9, 11, 12, 14, 23–25), were markedly increased in all of the SS-3 adenomas (Figs. 2 and 3). These genes and others identified by our analysis are involved in a number of altered genetic pathways including cellular proliferation, angiogenesis, and local T-cell immune response regulation in other cancers (Table 2). Because drugs targeting the components of these pathways are already available or in clinical trials, our results raise the possibility that these drugs may prove to be effective in some patients with invasive SS-3 adenomas. It should be kept in mind that this type of canonical pathway analysis does not necessarily detect all relevant signaling pathways, and genetic and epigenetic alterations such as the methylation profile at the genomic level would not be captured by this pathway analysis. In addition, subsequent immunohistochemical staining for CD3 demonstrated a smaller number of tumor infiltrating lymphocytes in the SS-3 group versus the NC group (Fig. 4; Table 3), which may reflect the differential expression of T-cell influencing genes.

Methods by which tumor cells escape from or actively suppress immune surveillance are active areas of investigation (26). This process has been divided into 3 phases: elimination, in which the immune system is able to recognize and eliminate tumor or pretumor cells; equilibrium, in which the immune system is able to prevent the tumor from growing or metastasizing; and escape, in which the tumor cells have developed mechanisms for evading the immune system and the tumor is

**TABLE 2.** Most Significant ($p < 0.01$; Adjusted for Multiple Comparisons) Canonical Pathway Alterations Identified Between SS-3 and NC Tumor Groups

| Pathway | Pathway Name* | Pathway Member Genes Altered in SS-3 Tumors | p-value** | Z-score |
|---|---|---|---|---|
| 1 | p53 Signaling | *SNAI2*,**GADD45G,PIK3R1,PLAGL1**,*PIK3C2G,FGFR2,SERPINE2* | 6.76E-05 | Increased |
| 2 | Nitric Oxide Signaling in the Cardiovascular System | *VEGFA,FLT1*,**PIK3R1,***PIK3C2G,FGFR2*,**ARG2,***PDE1C* | 7.59E-05 | *Decreased* |
| 3 | VEGF Family Ligand-Receptor Interactions | *VEGFA,FLT1*,**PIK3R1**,*PIK3C2G,FGFR2,PLA2G2A* | 0.00015 | *Decreased* |
| 4 | 3-phosphoinositide Biosynthesis | **MET**,*TNS3*,**PIK3R1**,*PIK3C2G,FGFR2*,**EYA4,PPFIA2**,*DUSP2* | 0.00047 | Undefined*** |
| 5 | Relaxin Signaling | *VEGFA*,**PIK3R1**,*PIK3C2G,FGFR2*,**ADCY8**,*PDE6B,PDE1C* | 0.00051 | *Decreased* |
| 6 | eNOS Signaling | *VEGFA,FLT1*,**PIK3R1**,*PIK3C2G,FGFR2*,**ADCY8**,*ESR1* | 0.00085 | *Decreased* |
| 7 | Axonal Guidance Signaling | **MET**,*VEGFA*,**SEMA3A**,*PAPPA,EPHA8*,**PIK3R1,** *UNC5B,PIK3C2G,FGFR2,HHIP*,**ROBO2**,*BMP5* | 0.00087 | Undefined |
| 8 | G-Protein Coupled Receptor Signaling | *MC3R*,**PIK3R1,CNR1**,*PIK3C2G,FGFR2*,**ADCY8,** **AVPR1B**,*PDE6B,PDE1C* | 0.00087 | Undefined |
| 9 | Renal Cell Carcinoma Signaling | **MET,***VEGFA*,**PIK3R1,***PIK3C2G,FGFR2* | 0.00093 | Undefined |
| 10 | Leptin Signaling in Obesity | **PIK3R1**,*PIK3C2G,GHSR,FGFR2*,**ADCY8** | 0.0011 | Undefined |
| 11 | Arginine Degradation VI (Arginase 2 Pathway) | **ARG2,PYCR1** | 0.0012 | Undefined |
| 12 | IL-4 Signaling | ***HLA-DRB1***,**PIK3R1,***HLA-B*,*PIK3C2G,FGFR2* | 0.0013 | Undefined |
| : | | | | |
| 20 | iCOS-iCOSL Signaling in T Helper Cells | ***HLA-DRB1***,**PIK3R1,***HLA-B*,*PIK3C2G,FGFR2* | 0.0069 | *Decreased* |
| : | | | | |
| 28 | Role of NFAT in Regulation of the Immune Response | ***HLA-DRB1***,**PIK3R1,***HLA-B*,*PIK3C2G,FGFR2*,**RCAN2** | 0.0069 | *Decreased* |
| 29 | CD28 Signaling in T Helper Cells | ***HLA-DRB1***,**PIK3R1,***HLA-B*,*PIK3C2G,FGFR2* | 0.0071 | Undefined |
| 30 | PKC$\theta$ Signaling in T Lymphocytes | ***HLA-DRB1***,**PIK3R1,***HLA-B*,*PIK3C2G,FGFR2* | 0.0072 | *Decreased* |
| : | | | | |
| 32 | Th1 Pathway | ***HLA-DRB1***,**PIK3R1,***HLA-B*,*PIK3C2G,FGFR2* | 0.0078 | *Decreased* |

Bold = increased; italic = decreased; underlined = genes involved in genetic pathways including cellular proliferation, angiogenesis, and local T-cell immune response regulation in other cancers.

*Pathway names are derived from their originally identified functions and do not necessarily correspond to their function in these adenomas.

**p-values corrected for multiple comparisons.

***Modeling was able to predict gene associations but not overall pathway direction.

able to expand (27, 28). A variety of different genes have been implicated in the modulation of the tumor microenvironment and subsequent escape from T-cell mediated immunosurveillance in a variety of different tumors, including melanoma, multiple myeloma, neuroblastoma, prostate cancer, breast cancer, and various sarcomas (23, 25, 26, 29, 30).

Recently, the secreted molecule arginase-II (ARG2), which converts L-arginine to L-ornithine and urea in the final step of the urea cycle (31), has been implicated in the inhibition of immune surveillance. It has been shown that high concentrations of ARG2 are often present both systemically and in the tumor microenvironment of various cancer types, resulting in reduction of arginine and suppression of T-cell function. Therefore, ARG2 is a plausible therapeutic target, and, indeed, arginase inhibitors have already been used clinically for other conditions (25, 30).

Similarly, the gene product of *SEMA3A*, semaphorin 3 A (SEMA3A), has a potential local immunosuppressive function in neoplastic conditions. Secreted under normal conditions by T-cells as part of a negative feedback loop and aberrantly by some tumor cells, SEMA3A acts on neuropilin-1 (NP-1) to suppress T-cell proliferation and function, a process that has been positively correlated with tumor invasion and metastasis (14). Studies have demonstrated that this SEMA3A-NP-1 interaction blocks cytoskeleton reorganization in T-cells and inhibits T-cell receptor signaling in vivo, and that the inhibition of SEMA3A significantly restores T-cell proliferation in vitro (12).

HLA class I proteins, including HLA-B, are expressed on all nucleated cells to present antigen to circulating cytotoxic T-cells (10, 13). Many types of cancer cells have been demonstrated to selectively downregulate HLA proteins (effectively hiding tumor antigens from cytotoxic T-cells) as a strategy to avoid immune system detection (10, 13, 32–36). Multiple studies have shown that downregulation or loss of HLA signaling proteins on the cell surface of tumor cells is associated with a significantly worse outcome in a wide variety of cancer types (10, 33, 37).

By depleting the local environment of arginine needed for T-cell function and preventing T-cell proliferation and signaling through interaction with NP-1, respectively, ARG2 and SEMA3A act to inhibit the function of adjacent T-cells. By downregulating HLA-B, the tumor cells may also be able to avoid detection by any cytotoxic T-cells present (10, 13).

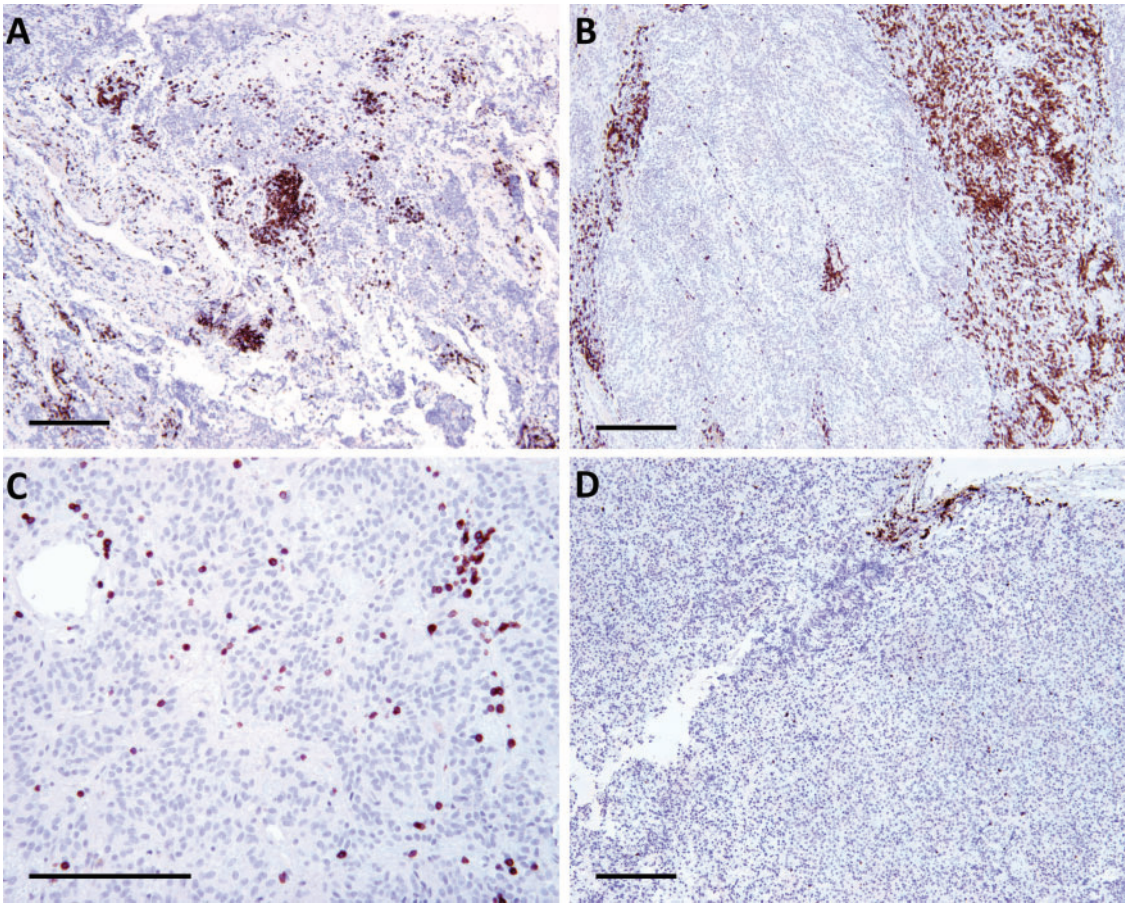


**FIGURE 4.** Immunohistochemistry for CD3 in cases of null cell pituitary adenomas demonstrating +++ **(A, B)** and ++ **(C)** tumor infiltrating lymphocyte (TIL) levels in null cell cases and + TIL levels in a silent subtype III case **(D)**. Magnifications: **A, B, D** = 40×; **C** = 100×. Scale bars: 200 μm.

**TABLE 3.** Relative Quantification of CD3+ Lymphocytes

| Null Cell Cases | | Silent-Subtype III Cases | |
|---|---|---|---|
| **Patient** | **CD3+ Lymphocytes** | **Patient** | **CD3+ Lymphocytes** |
| 1 | +++ | 5 | + |
| 2 | ++ | 6 | − |
| 3 | + | 7 | + |
| 4 | ++ | 8 | + |
| **Additional Null Cell Cases** | | **Additional SS-3 Cases** | |
| A1 | + | A11 | − |
| A2 | ++ | A12 | + |
| A3 | ++ | A13 | ++ |
| A4 | + | A14 | + |
| A5 | +++ | A15 | − |
| A6 | ++ | A16 | + |
| A7 | + | A17 | ++ |
| A8 | + | A18 | + |
| A9 | +++ | A19 | − |
| A10 | ++ | A20 | − |

The altered levels of these 3 gene products may act synergistically at multiple levels of the cell mediated immune response to suppress the proliferation, metabolic activity, and function of T-cells, allowing the tumor to escape the immune surveillance pathway and grow unchecked in a manner unavailable to conventional null cell adenomas (27, 28, 38). Our qualitative finding that there is a generalized decrease in infiltrating T-cells in the SS-3 group seems to support the hypothesis that the altered mRNA levels of *ARG2*, *SEMA3A*, and *HLA-B* may act to inhibit T-cell presence and activity within these tumors. ARG2 and SEMA3A are potentially targetable molecules, as inhibitors are currently being investigated in in vivo and in vitro studies (12, 30) and could allow for normalization of T-cell proliferation and activity.

This study is also a further validation of our previously described method for differentiating SS-3 adenomas from conventional null cell adenomas using GLG-1 immunohistochemistry (4) (Supplementary Data Fig. S1), as it demonstrates that there is indeed a qualitative and quantitative difference in mRNA expression patterns between these 2 tumor types

(Figs. 1–3) and suggests a potential mechanism for increased aggressiveness in the SS-3 cohort. However, it is unclear if the increased production of these mRNA species in SS-3 compared with NC adenomas fully explains the enlargement and fragmentation of the Golgi apparatus in SS-3 adenomas.

In conclusion, this RNA analysis suggests a potentially targetable mechanism for the previously observed aggressive behavior of SS-3 adenomas (2, 4, 5). By downregulating the expression of antigen-presenting molecules and upregulating the expression of secreted proteins that inhibit the metabolism, function, and proliferation of local cytotoxic T-cells, these tumors can escape from immune surveillance and thus may grow more rapidly and recur more frequently.

## ACKNOWLEDGMENT

*The authors would like to thank Niccole Williams, Agatha Villegas, and Antonio Atkins for excellent administrative professional services.*

## REFERENCES

1. Horvath E, Kovacs K, Killinger DW, et al. Silent corticotropic adenomas of the human pituitary gland: A histologic, immunocytologic, and ultrastructural study. Am J Pathol 1980;98:617–38
2. Horvath E, Kovacs K, Smyth HS, et al. A novel type of pituitary adenoma: Morphological features and clinical correlations. J Clin Endocrinol Metab 1988;66:1111–8
3. Mete O, Gomez-Hernandez K, Kucharczyk W, et al. Silent subtype 3 pituitary adenomas are not always silent and represent poorly differentiated monomorphous plurihormonal Pit-1 lineage adenomas. Mod Pathol 2016;29:131–42
4. Richardson TE, Mathis DA, Mickey BE, et al. Clinical outcome of silent subtype III pituitary adenomas diagnosed by immunohistochemistry. J Neuropathol Exp Neurol 2015;74:1170–7
5. Erickson D, Scheithauer B, Atkinson J, et al. Silent subtype 3 pituitary adenoma: A clinicopathologic analysis of the Mayo Clinic experience. Clin Endocrinol (Oxf) 2009;71:92–9
6. Scheithauer BW, Kovacs KT, Laws ER, et al. Pathology of invasive pituitary tumors with special reference to functional classification. J Neurosurg 1986;65:733–44
7. Ebersold MJ, Quast LM, Laws ER, et al. Long-term results in transsphenoidal removal of nonfunctioning pituitary adenomas. J Neurosurg 1986;64:713–9
8. Di Ieva A, Rotondo F, Syro LV, et al. Aggressive pituitary adenomas: Diagnosis and emerging treatments. Nat Rev Endocrinol 2014;10:423–35
9. Bronte V, Zanovello P. Regulation of immune responses by L-arginine metabolism. Nat Rev Immunol 2005;5:641–54
10. Chang CC, Ferrone S. Immune selective pressure and HLA class I antigen defects in malignant lesions. Cancer Immunol Immunother 2007;56:227–36
11. Geiger R, Rieckmann JC, Wolf T, et al. L-Arginine modulates T cell metabolism and enhances survival and anti-tumor activity. Cell 2016;167:829–42 (e13)
12. Lepelletier Y, Moura IC, Hadj-Slimane R, et al. Immunosuppressive role of semaphorin-3A on T cell proliferation is mediated by inhibition of actin cytoskeleton reorganization. Eur J Immunol 2006;36:1782–93
13. Seliger B. Different regulation of MHC class I antigen processing components in human tumors. J Immunotoxicol 2008;5:361–7
14. Takamatsu H, Okuno T, Kumanogoh A. Regulation of immune cell responses by semaphorins and their receptors. Cell Mol Immunol 2010;7:83–8
15. Going JJ. Counting cells made easier. Histopathology 2006;49:309–11
16. Aronesty E. Comparison of sequencing utility programs. Open Bioinformatics J 2013;7:1–8
17. Kim D, Pertea G, Trapnell C, et al. TopHat2: Accurate alignment of transcriptomes in the presence of insertions, deletions and gene fusions. Genome Biol 2013;14:R36
18. Liao Y, Smyth GK, Shi W. featureCounts: An efficient general purpose program for assigning sequence reads to genomic features. Bioinformatics 2014;30:923–30
19. Robinson MD, McCarthy DJ, Smyth GK. edgeR: A Bioconductor package for differential expression analysis of digital gene expression data. Bioinformatics 2010;26:139–40
20. Taboada GF, Luque RM, Bastos W, et al. Quantitative analysis of somatostatin receptor subtype (SSTR1-5) gene expression levels in somatotropinomas and non-functioning pituitary adenomas. Eur J Endocrinol 2007;156:65–74
21. Shen ZJ, Braun RK, Hu J, et al. Pin1 protein regulates Smad protein signaling and pulmonary fibrosis. J Biol Chem 2012;287:23294–305
22. Guo X, Fan Y, Lang R, et al. Tumor infiltrating lymphocytes differ in invasive micropapillary carcinoma and medullary carcinoma of breast. Modern Pathol 2008;21:1101–7
23. Gannon PO, Godin-Ethier J, Hassler M, et al. Androgen-regulated expression of arginase 1, arginase 2 and interleukin-8 in human prostate cancer. PLoS One 2010;5:e12107
24. Mussai F, De Santo C, Abu-Dayyeh I, et al. Acute myeloid leukemia creates an arginase-dependent immunosuppressive microenvironment. Blood 2013;122:749–58
25. Mussai F, Egan S, Hunter S, et al. Neuroblastoma arginase activity creates an immunosuppressive microenvironment that impairs autologous and engineered immunity. Cancer Res 2015;75:3043–53
26. Swann JB, Smyth MJ. Immune surveillance of tumors. J Clin Invest 2007;117:1137–46
27. Dunn GP, Old LJ, Schreiber RD. The three Es of cancer immunoediting. Annu Rev Immunol 2004;22:329–60
28. Dunn GP, Old LJ, Schreiber RD. The immunobiology of cancer immunosurveillance and immunoediting. Immunity 2004;21:137–48
29. Swann JB, Hayakawa Y, Zerafa N, et al. Type I IFN contributes to NK cell homeostasis, activation, and antitumor function. J Immunol 2007;178:7540–9
30. Pistoia V, Morandi F, Bianchi G, et al. Immunosuppressive microenvironment in neuroblastoma. Front Oncol 2013;3:167
31. Wu G, Morris SM, Arginine metabolism: Nitric oxide and beyond. Biochem J 1998;336:1–17
32. Aptsiauri N, Cabrera T, Garcia-Lora A, et al. MHC class I antigens and immune surveillance in transformed cells. Int Rev Cytol 2007;256:139–89
33. Aptsiauri N, Cabrera T, Mendez R, et al. Role of altered expression of HLA class I molecules in cancer progression. Adv Exp Med Biol 2007;601:123–31
34. Garrido F, Cabrera T, Concha A, et al. Natural history of HLA expression during tumour development. Immunol Today 1993;14:491–9
35. Hicklin DJ, Marincola FM, Ferrone S. HLA class I antigen downregulation in human cancers: T-cell immunotherapy revives an old story. Mol Med Today 1999;5:178–86
36. Vertuani S, Triulzi C, Roos AK, et al. HER-2/neu mediated downregulation of MHC class I antigen processing prevents CTL-mediated tumor recognition upon DNA vaccination in HLA-A2 transgenic mice. Cancer Immunol Immunother 2009;58:653–64
37. Kaneko K, Ishigami S, Kijima Y, et al. Clinical implication of HLA class I expression in breast cancer. BMC Cancer 2011;11:454
38. Dunn GP, Bruce AT, Ikeda H, et al. Cancer immunoediting: From immunosurveillance to tumor escape. Nat Immunol 2002;3:991–8